Flood Radar: Multi-Sensor SAR-Based Flood Mapping and Evacuation Modeling -

A Case Study of the July 2025 Texas Flood

Antonika Shapovalova¹,

¹NASA Earth Science Applied Sciences Program, USA

This is a non-peer-reviewed preprint submitted to EarthArXiv.

The content has not undergone formal peer review.

If a version of record is later published, its DOI and citation will be added here.

Flood Radar: Multi-Sensor SAR-Based Flood Mapping and Evacuation Modeling - A Case
Study of the July 2025 Texas Flood

Antonika Shapovalova

October 2025

Abstract

Floods remain among the most destructive natural hazards worldwide, causing an average of USD 40 billion in annual damage and affecting more than 2.5 billion people between 1994 and 2014. The Central Texas flood of July 2025 was one of the most catastrophic in recent decades, triggered by the remnants of Tropical Storm Barry that delivered over 508 mm of rain within two days. This study presents Flood Radar, an integrated multi-sensor system designed for near-real-time flood mapping and evacuation planning, demonstrated through this extreme event. The system combines C-band Sentinel-1 synthetic aperture radar (SAR) data, L-band UAVSAR and ALOS-2/PALSAR-2 imagery, NASA GPM IMERG precipitation fields, and digital elevation models (SRTM and Copernicus DEM) with infrastructure layers from OpenStreetMap. Standardized preprocessing, including orbit correction, radiometric calibration, speckle filtering, and DEM-assisted geocoding, prepares inputs for a pretrained deep-learning segmentation model (U-Net/FCN) that classifies water and land surfaces at 10 m resolution. Change-detection and hydrodynamic modeling using HEC-RAS further estimate water depth, flow velocity, and potential road inundation.

The resulting flood-extent maps accurately delineated both open and sub-canopy inundation zones, revealing the rapid ≈ 9.8 m rise of the Guadalupe River and identifying ~ 740 acres of flooded cropland and pasture in Kerr County. Integration with OpenStreetMap enabled automatic evaluation of road passability and generation of optimal evacuation routes. The public web interface (https://evacuation-map-sar.vercel.app/) demonstrates the operational output of the system. The study highlights the advantages of multi-sensor fusion, SAR's cloud-independent imaging, L-band's vegetation penetration, and near-continuous IMERG rainfall monitoring, while noting limitations such as speckle noise, sparse revisit intervals, and misclassification in urban

environments. The July 2025 case underscores the necessity of coupling advanced Earthobservation tools with effective early-warning and communication systems. Flood Radar
exemplifies a scalable framework for rapid disaster intelligence that supports timely evacuation
and post-event recovery planning in flood-prone regions.

Keywords

Flood mapping; synthetic aperture radar (SAR); Sentinel-1; UAVSAR; ALOS-2 PALSAR-2; GPM IMERG; HEC-RAS; Copernicus DEM; SRTM; multi-sensor integration; deep learning; U-Net segmentation; Central Texas flood 2025; OpenStreetMap; evacuation modeling; disaster response.

Introduction

Floods are among the most consequential natural hazards worldwide, driving substantial human and economic losses. Recent syntheses estimate average annual damages on the order of \$40 billion (2015 USD), with more than 2.5 billion people affected between 1994 and 2014, figures that underscore the need for timely, objective situational awareness during fast-evolving events(1).

Central Texas is particularly vulnerable: the steep, karstic terrain and shallow soils of the Hill Country, often referred to as "Flash Flood Alley", promote rapid runoff and explosive river responses when intense convection stalls over the region(2).

During 4–7 July 2025, a quasi-stationary mesoscale convective episode delivered extreme rainfall across the Hill Country, producing rapid rises on the Guadalupe River (32 ft in 1.5–1.75 h at Kerrville and Comfort) and widespread damage. The confirmed death toll ultimately exceeded 130 statewide, making this one of the deadliest non-tropical flash-flood disasters in modern U.S. records; preliminary economic-loss estimates range from \$1.1 billion in residential damage to \$18–22 billion in total regional impacts.

These dynamics highlight a central operational challenge: actionable flood maps must be produced within hours under heavy cloud cover and often at night.

Spaceborne synthetic aperture radar (SAR) is well-suited to this task because it acquires data independent of illumination and cloud cover, offers meter-to-tens-of-meters spatial detail, and encodes scattering mechanisms that help discriminate open water and inundated vegetation. Deep convolutional models (e.g., U-Net/FCN) have further advanced pixel-level flood delineation, typically outperforming classical thresholding in accuracy and robustness. Complementary L-band observations (e.g., UAVSAR, ALOS-2/PALSAR-2) enhance detection beneath canopies via double-bounce scattering, improving boundary realism in vegetated floodplains(3).

This paper presents Flood Radar, an integrated, near-real-time workflow that fuses C-band Sentinel-1 SAR with ancillary datasets - NASA GPM IMERG precipitation (0.1°/30 min), Copernicus DEM topography, and OpenStreetMap infrastructure, augmented by targeted L-band airborne acquisitions when available. The system automates SAR pre-processing, semantic water segmentation, and change detection, then ingests precipitation and elevation constraints to refine inundation masks and support evacuation-route analysis. We evaluate Flood Radar on the July 2025 Central Texas floods, with four objectives: (1) characterize the strengths and limits of SAR-based flood mapping; (2) document the end-to-end automation for rapid products; (3) quantify infrastructure and agricultural impacts; and (4) demonstrate how multi-sensor fusion can inform life-safety decisions during flash-flood crises(4-6).

Collectively, the results illustrate how operational SAR, precipitation satellites, and open elevation/transport data can be combined to deliver decision-ready flood intelligence on time scales commensurate with emergency response.

Methods (SAR Data and Sources)

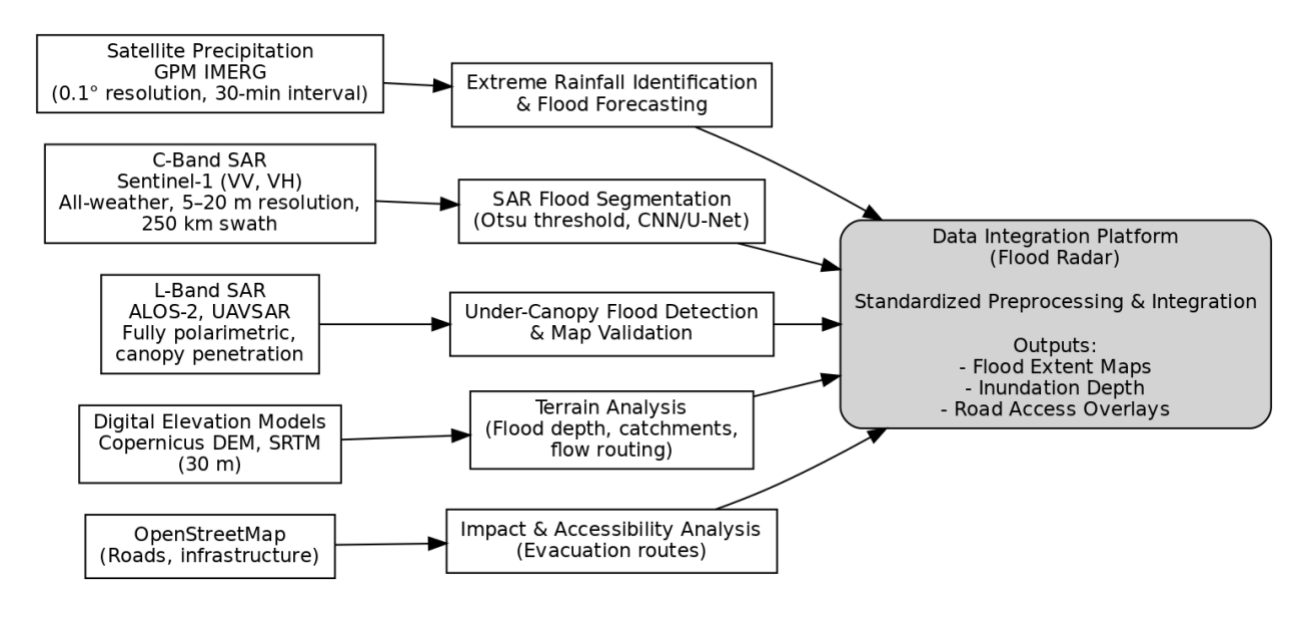


Figure 1: Flowchart illustrating how each dataset feeds into the flood mapping and analysis pipeline (Flood Radar platform). Satellite precipitation (GPM IMERG) data is analyzed for extreme rainfall identification and flood forecasting. C-band SAR imagery (Sentinel-1) undergoes threshold-based and deep learning segmentation to map surface water extents, while L-band SAR data (ALOS-2, UAVSAR) supports under-canopy flood detection and map validation using its penetration and polarimetric capabilities. Digital elevation models (Copernicus DEM, SRTM) enable terrain analysis for flood depth estimation, catchment delineation, and flow routing. OpenStreetMap layers (roads, infrastructure) support impact and accessibility analysis (e.g. evacuation route planning). All processed outputs are integrated on the Flood Radar platform (with standardized preprocessing) to produce final flood extent maps, inundation depth estimates, and road access overlays for emergency response.

Satellite Precipitation (GPM IMERG)

A key input for flood modeling is satellite-based rainfall data. We use the Integrated Multi-satellite Retrievals for GPM (IMERG) product, which provides quasi-global precipitation estimates at 0.1° spatial resolution (10 km) every 30 minutes(7). IMERG blends observations from numerous microwave radiometers and the TRMM/GPM missions to produce near-continuous rainfall maps, an especially valuable capability in regions lacking ground rain gauges. This allows us to track accumulated rainfall and identify extreme precipitation that could lead to flooding, forming the basis for flood forecasting in the Flood Radar system.

C-Band SAR Imagery (Sentinel-1)

For direct flood inundation mapping, we rely on C-band Synthetic Aperture Radar (SAR) imagery from the Sentinel-1 satellite constellation. Sentinel-1 provides high-resolution (~5–20 m) observations with a frequent revisit (6–12 days globally with two satellites) and a wide swath (up to 250 km), and it operates day or night in all-weather conditions(8). These characteristics make Sentinel-1 ideal for rapid flood mapping, as cloud cover or darkness do not hinder data acquisition. We utilize the Level-1 Ground Range Detected (GRD) products in dual polarization (VV and VH), which have proven effective for distinguishing water from land. In particular, the VV channel is sensitive to surface water roughness (calm water appears dark) while the cross-polarized VH

channel captures volume scattering from vegetation; together, they provide complementary information to detect inundation even in vegetated areas(8). This dual-polarization approach enables more robust and real-time separation of flooded versus dry surfaces in our analyses.

SAR Flood Mapping Techniques

Threshold-Based Segmentation

One approach for delineating flood extents from SAR imagery is classical threshold segmentation. We employ Otsu's method, a non-parametric algorithm that automatically determines the optimal backscatter threshold by maximizing the between-class variance of pixel intensities (water vs. non-water)(8). SAR images are first preprocessed following standard remotesensing procedures – including precise orbital correction, radiometric calibration, speckle noise reduction (e.g. using a Lee filter), and contrast enhancement via histogram equalization – before applying the thresholding(8). This yields an initial binary flood mask that can be produced rapidly for emergency mapping. However, simple threshold methods can misclassify areas due to noise or vegetation effects, necessitating further refinement.

Deep Learning Segmentation

We also investigate modern deep-learning methods to improve flood mapping accuracy. Convolutional neural network (CNN) based segmentation models (such as fully convolutional networks, U-Net, or Siamese CNNs operating on multi-temporal SAR inputs) can automatically learn discriminative features for water detection. A recent review of 58 studies found that models built on convolutional layers generally achieve higher accuracy than those with only fully-connected layers, as the convolutional architectures better exploit spatial patterns of flooding(9). These deep-learning models have been shown to outperform traditional thresholding in both detection accuracy and processing speed(9). Nonetheless, the same review highlighted outstanding

challenges: current models are usually deterministic and trained on specific events, so more work is required to improve their generalization to unseen floods and to account for prediction uncertainty in an operational context(9). In our project, we leverage CNN-based segmentation to complement threshold methods, aiming to combine the efficiency of thresholding with the adaptability of learning-based approaches.

L-Band SAR Sensors (ALOS-2 and UAVSAR)

To enhance flood mapping in forested or vegetated regions, we incorporate L-band SAR data, which penetrates vegetation more effectively. The JAXA ALOS-2 satellite (with its PALSAR-2 sensor) operates in the L-band microwave spectrum, which is less attenuated by clouds and heavy rainfall(10). L-band waves can partially penetrate tree canopies, improving flood detection under vegetation. ALOS-2 offers multiple imaging modes ranging from high-resolution Spotlight (3 × 1 m azimuth × range) to wide-area ScanSAR (100 m resolution), and it has both right-looking and left-looking observation capability for increased coverage frequency(11). The satellite's orbit cycle (approximately 14 days) allows a revisit of the same area about every two weeks(11), which is useful for capturing peak flood extent in remote regions. We use ALOS-2 data (when available) to refine the flood boundaries in areas where C-band signals may be obscured or attenuated by dense vegetation.

In addition to satellite data, we utilize NASA's UAVSAR airborne L-band radar for targeted high-resolution observations. UAVSAR is a fully polarimetric L-band SAR deployed on a Gulfstream III aircraft, designed for repeat-pass interferometry and high-precision imaging(12). It provides 2 m range resolution and a swath width over 16 km(12), and can be flown along the same flight path with meter-level precision. This allows near-exact revisits for "before-and-after" comparisons or time-series monitoring over flood-prone areas. Data from UAVSAR (when

available from airborne campaigns) are particularly valuable for capturing fine-scale flooding details, validating satellite-derived flood maps, and observing inundation beneath tree canopies. Notably, the fully polarimetric L-band data (HH, HV, VH, VV) can be decomposed to identify different scattering mechanisms. Such polarimetric analysis has been shown to yield the highest flood classification accuracy in vegetated terrain, as it distinguishes open water surfaces from water under vegetation by their scattering signatures(13). Therefore, integrating ALOS-2 and UAVSAR L-band observations helps ensure that Flood Radar can detect floods in a variety of land cover conditions, including forested wetlands and agricultural areas.

Digital Elevation Models (Copernicus DEM and SRTM)

Terrain data are incorporated to provide context on floodplain topography and to aid in modeling water flow and evacuation routes. We use the Copernicus Digital Elevation Model (Copernicus DEM), which is a global digital surface model derived from the TanDEM-X interferometric mission (data acquired 2011–2015)(5). The Copernicus DEM represents the Earth's surface including buildings and vegetation, and is available at 30 m (global, GLO-30) and 90 m (global, GLO-90) resolution worldwide (a 10 m DSM is available over Europe under the EEA-10 product)(5). Notably, this dataset has undergone extensive editing to improve its quality – for example, water bodies have been flattened and rivers adjusted to ensure consistent downstream flow(5). Such preprocessing makes the DEM more hydrologically sound for flood modeling. We leverage the Copernicus DEM to delineate catchment areas, estimate flood water depths (by subtracting DEM elevations from satellite-derived water surface heights, where available), and to identify terrain features that could impact flood extent or evacuation path planning.

We also utilize the Shuttle Radar Topography Mission (SRTM) DEM for comparison and supplemental coverage. SRTM flew aboard Space Shuttle Endeavour in February 2000 and produced the first near-global terrain dataset by mapping 80% of Earth's land surface between 60° N and 56° S(14). The mission used dual-frequency SAR (C-band and X-band) in a single-pass interferometer configuration to acquire elevation data. SRTM data were originally released at 1 arc-second (30 m) resolution for the United States and 3 arc-seconds (90 m) for areas outside the U.S.(14). (Subsequent releases have made the 30 m resolution data globally available, after void-filling.) In our project, the SRTM (typically the 30 m version) serves as an additional elevation reference – for instance, to cross-check the Copernicus DEM in regions where they overlap, or to use in flood simulations and routing algorithms where a coarser but globally consistent DEM is sufficient. Together, the high-resolution Copernicus DEM and the SRTM provide critical topographic information for understanding flood dynamics (e.g., identifying flow paths, depressions, and potential natural barriers) and for determining optimal evacuation routes that avoid low-lying flooded areas.

Road Network Data (OpenStreetMap)

For evacuation modeling, up-to-date road network and infrastructure data are essential. We integrate open map data from the OpenStreetMap (OSM) project – often referred to as the "Wikipedia of maps" due to its crowdsourced, collaborative nature(15). OSM provides a freely available, community-updated map of the world's roads, highways, and critical infrastructure, released under the Open Database License (ODbL) which permits free use and sharing of the data(15). These data have been widely used in humanitarian contexts; the Humanitarian OpenStreetMap Team (HOT) in particular has a history of mobilizing volunteers to map disaster-affected regions. HOT's first activation was in 2009 to map the Gaza Strip, and OSM data saw

extensive use during the Haiti 2010 earthquake response, when within days volunteers had created the most detailed map of Haiti to assist relief efforts(15). In the Flood Radar system, we use OSM road and infrastructure layers in conjunction with the SAR-derived flood maps. This enables us to identify which road segments are inundated or likely impassable, to estimate accessibility of certain areas, and to suggest alternative evacuation routes that circumvent flooded zones. By overlaying flood extents on the road network, responders can quickly see which towns or communities have lost road access and can plan relief logistics or evacuations accordingly. The open-source nature of OSM ensures that this information can be updated in real time by local contributors as conditions evolve.

Data Integration and Processing

All the aforementioned datasets are processed and combined within a unified Flood Radar platform. Each data source undergoes standardized preprocessing to ensure compatibility: satellite scenes are georeferenced to a common coordinate system and grid, SAR images are calibrated and despeckled, and all raster data (SAR, precipitation, DEMs) are resampled to consistent spatial scales as needed. The multi-source data integration allows cross-validation and enrichment of the flood analysis — for example, rainfall intensity peaks from IMERG can be correlated with downstream flood detections in SAR images, and low-lying areas in the DEM can be flagged as high flood-risk zones even before waters arrive. By fusing C-band and L-band SAR observations, we capture both broad inundation patterns and flooded areas under vegetation. The quantitative precipitation data help estimate flood onset and potential severity, while the DEM underpins water depth estimation and flow modeling. Finally, the road network overlay supports translating flood maps into actionable information for emergency management, such as identifying communities at risk of being isolated and planning safe evacuation corridors. This integrated approach provides a

robust, objective basis for decision-making during floods – allowing responders to assess flood extent, depth, and evolution over time, to estimate impacts (e.g. on agriculture or infrastructure), and to optimize evacuation and relief routes using the best available remote sensing and open data.

Data and Processing

Remote Sensing Data and Preprocessing

Satellite SAR Data

To establish a baseline water extent and capture flood conditions, we collected Sentinel-1 C-band SAR images from before and after the July 2025 flood. Specifically, pre-event scenes from June 1 – July 1, 2025 and post-event scenes from July 3 – 14, 2025 were used(16), aligning with the USDA NASS flood assessment timeframe. Each Sentinel-1 scene provides dual polarization (VV and VH) amplitude data in Ground Range Detected (GRD) format.

SAR Preprocessing

We applied standard SAR preprocessing steps to convert the raw Sentinel-1 data into analysis-ready backscatter images. This included applying precise orbit corrections, removing thermal noise and borderline artifacts, performing radiometric calibration to sigma-nought, and geometrically correcting for terrain (using a Digital Elevation Model) with speckle noise filtering(17). These steps eliminate orbital and geometric distortions, normalize the backscatter values for physical consistency, and reduce the salt-and-pepper speckle, thereby improving the accuracy of subsequent water classification. All SAR images were projected onto a common map grid (UTM Zone 14N) during terrain correction to ensure alignment across dates.

Additional L-band SAR

To better detect flooding under vegetation canopies, we incorporated L-band SAR data from ALOS-2/PALSAR-2 and NASA's airborne UAVSAR. L-band microwaves penetrate foliage more effectively than C-band, helping identify inundation in forested or vegetated areas. ALOS-2/PALSAR-2 operates in multiple modes – e.g. stripmap modes with 3 m (Ultra-Fine), 6 m, and 10 m resolution, and a ScanSAR mode (100 m) – and even offers a spotlight mode achieving 1 × 3 m resolution(10). The UAVSAR airborne radar is a fully polarimetric L-band system with an 80 MHz bandwidth giving 2 m range resolution and a swath width >16 km; it uses precision GPS navigation to fly repeat passes within 10 m of the same track, enabling detailed change detection(12). These L-band datasets were used to refine flood boundary mapping in densely vegetated regions where C-band alone might miss under-story water.

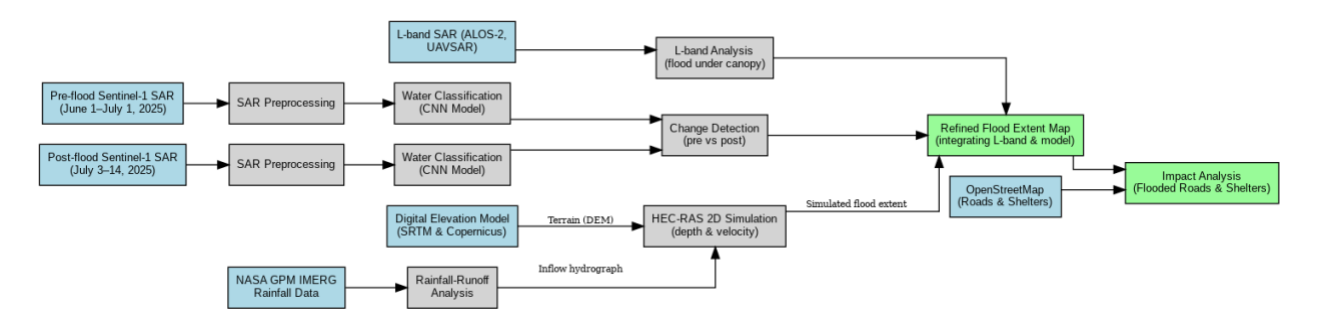


Figure 2: Data and processing workflow for the July 2025 Central Texas flood mapping. Multisource inputs (Sentinel-1 C-band SAR pre- and post-flood images, L-band SAR from ALOS-2 and UAVSAR, GPM IMERG rainfall estimates, high-resolution DEM, and OpenStreetMap infrastructure data) feed into the flood mapping pipeline. Sentinel-1 images are preprocessed (orbit correction, noise removal, calibration, terrain correction) and then passed through a CNN-based water classification model to generate pre-event and post-event water masks. Change detection between these water masks yields an initial flooded area extent. L-band SAR data are analyzed to reveal inundation under vegetation canopies, which, along with the flood extent simulated by a HEC-RAS 2D hydrodynamic model (driven by rainfall-runoff-derived inflow and terrain data), are integrated with the Sentinel-1 results to refine the flood extent boundaries. The final flood inundation map (with extent and depth information) is overlaid on OSM roads and shelter locations to identify flooded roads, isolated communities, and at-risk critical facilities, supporting evacuation planning and emergency response.

Rainfall and Elevation Data

Precipitation Data

We analyzed rainfall antecedent to and during the flood using NASA's Global Precipitation Measurement (GPM) IMERG products. IMERG (Integrated Multi-satellite Retrievals) combines observations from a constellation of satellites to estimate precipitation over most of the Earth, including remote areas lacking ground rain gauges(4). It provides quasi-global rainfall intensity maps at 0.1° latitude/longitude resolution (10 km) with a 30-minute temporal frequency(18). We used the half-hourly IMERG data to capture the spatiotemporal distribution of the extreme July 2025 rainfall. Notably, IMERG is available in near real-time, updating every 30 minutes(4), which makes it well-suited for operational flood monitoring. The satellite-derived precipitation estimates allowed us to identify rainfall peaks and their coincidence with observed flooding, even in areas without ground stations.

Terrain Data (DEM)

Accurate topography is essential for flood mapping and hydrodynamic modeling. We compiled a high-resolution Digital Elevation Model (DEM) from two sources. First, we used the Shuttle Radar Topography Mission (SRTM) DEM, which provides 30 m horizontal resolution (1 arc-second) over the United States (and 90 m globally). SRTM data cover about 80% of the Earth's land surfaces between 60° N and 56° S(19), with the U.S. dataset at 1 arc-second and international data often resampled to 3 arc-seconds(19). Second, we incorporated the Copernicus DEM (an updated DSM derived from the TanDEM-X interferometric mission). The Copernicus DEM offers resolutions of 10 m (for Europe), 30 m, and 90 m globally(5). It is an edited DSM (branded WorldDEMTM) with corrections such as flattened water bodies and consistent river elevations to improve hydrological accuracy(5). By merging these sources, we obtained a seamless terrain

model with 10–30 m detail for Central Texas. This DEM was used both for geocoding SAR images and as input to flood simulations.

Infrastructure Data (Roads and Shelters)

To support evacuation planning and impact analysis, we extracted up-to-date infrastructure and population shelter data from OpenStreetMap (OSM). OSM is an open, crowdsourced mapping platform that is continuously updated by volunteer contributors, and it has proven to be a valuable data source for disaster management and risk assessment(20). From OSM, we obtained vector layers for the road network, as well as points of interest such as schools, churches, and other buildings that could serve as shelters or critical facilities. These data enable analysis of which roads might be flooded or which populated areas might be isolated. There are documented cases of OSM data being used extensively in disaster response efforts – for example, in the 2010 Haiti earthquake, the 2010 Pakistan floods, and the 2015 Nepal earthquake, volunteer mappers rapidly updated OSM to aid crisis response(20). Given this track record, integrating OSM layers into our flood mapping allowed us to identify inundated roads and accessible evacuation routes, and to pinpoint communities (and potential shelter sites) at risk.

Flood Extent Detection and Change Analysis

Water Classification via Deep Learning

We employed a pre-trained convolutional neural network (CNN) model to detect water in the SAR images. The model (sourced from Esri's Living Atlas repository) was originally trained on a large sample of Sentinel-1 SAR and Sentinel-2 optical imagery to recognize water bodies. We applied this model to each Sentinel-1 scene by tiling the scene into manageable patches ("chips") and generating a probability map of water vs. non-water for each pixel. Modern approaches to flood mapping favor such semantic segmentation models based on CNNs (e.g. U-

Net or Fully Convolutional Network architectures) to classify imagery at the pixel level. These methods leverage spatial context and learned features, and they typically outperform simple threshold-based classification (like Otsu's method) in both accuracy and robustness(21). In our case, the CNN water classifier provided an initial binary water mask for each pre-flood and post-flood scene, capturing rivers, reservoirs, and newly inundated areas with higher fidelity than a static backscatter threshold would.

Change Detection

To isolate the new flooding triggered by the July 2025 event, we performed a change detection analysis between the post-event and pre-event water masks. Specifically, we compared the flood period water extent (early July) against the baseline water extent from June. Pixels classified as water post-event but as land pre-event were flagged as flooded. This change detection approach is a common technique in SAR flood mapping: by differencing binary water maps (or using ratio metrics on the SAR backscatter), one can highlight newly inundated areas(21). We implemented a "water mask differencing" strategy, which is analogous to computing image differences or log-ratios of backscatter to detect flood-induced changes (21). To improve reliability, we utilized multiple pre-flood scenes (over the month prior) to ensure that persistent water bodies (e.g. permanent lakes) and noisy speckle variations would not be misclassified as new floods. Using a time series of several pre-event images helps filter out false positives by requiring that a pixel be consistently non-water before the event to be counted as flooded, a technique supported in prior studies(21). The output of this step was an inundation map delineating the extent of floodwaters in Central Texas, which we could overlay on the DEM and OSM layers for further analysis.

Hydrodynamic Simulation (HEC-RAS)

To estimate flood depths and flow velocities – critical parameters for assessing flood severity – we ran simulations with the Hydrologic Engineering Center's River Analysis System (HEC-RAS). HEC-RAS is a widely used hydrodynamic modeling software developed by the US Army Corps of Engineers, capable of one-dimensional and two-dimensional flood routing. It is known for its high accuracy in predicting water surface elevations and inundation extents even with limited input data(22). In fact, HEC-RAS is often regarded as one of the best tools for flood inundation mapping in research and practice(22).

We configured a HEC-RAS model for the affected river basins using the processed DEM as the terrain. Key model inputs included the river channel geometry (extracted from the DEM and available cross-section data), estimated inflow hydrographs (based on rainfall-runoff considerations and gauge data, if available), and land cover-based roughness coefficients (Manning's n values) for different surface types. The simulation was run in unsteady 2D flow mode over the flood period. HEC-RAS utilizes the Manning equation and shallow water flow equations to compute the depth and velocity of floodwaters at each grid cell. After calibration, the model produced maps of maximum water depth and flow velocity across the floodplain. We then intersected these outputs with the inundation extent (from SAR analysis) to validate and refine the flood extent boundaries. The resulting flood depth map was used to highlight the most severely flooded areas and to infer which roads or structures might have been submerged. By combining the satellite-derived flood extent with HEC-RAS's flow dynamics, our integrated Flood Radar system provides a comprehensive view of the event – identifying not only where flooding occurred, but also the flood's intensity (depth/velocity) at each location. This information is invaluable for emergency response planning and evacuation, as it enables authorities to prioritize high-danger zones and safe corridors.

Overall, the fusion of multi-source data – Sentinel-1 C-band imagery, L-band SAR for vegetated regions, IMERG rainfall estimates, high-resolution DEMs, and OSM infrastructure layers – underpins a robust flood mapping and modeling workflow. The described preprocessing, segmentation, and change detection steps form the core of our Flood Radar methodology, which delivered rapid and high-detail flood inundation maps for the July 2025 Central Texas event to support timely disaster response and evacuation planning.

Results

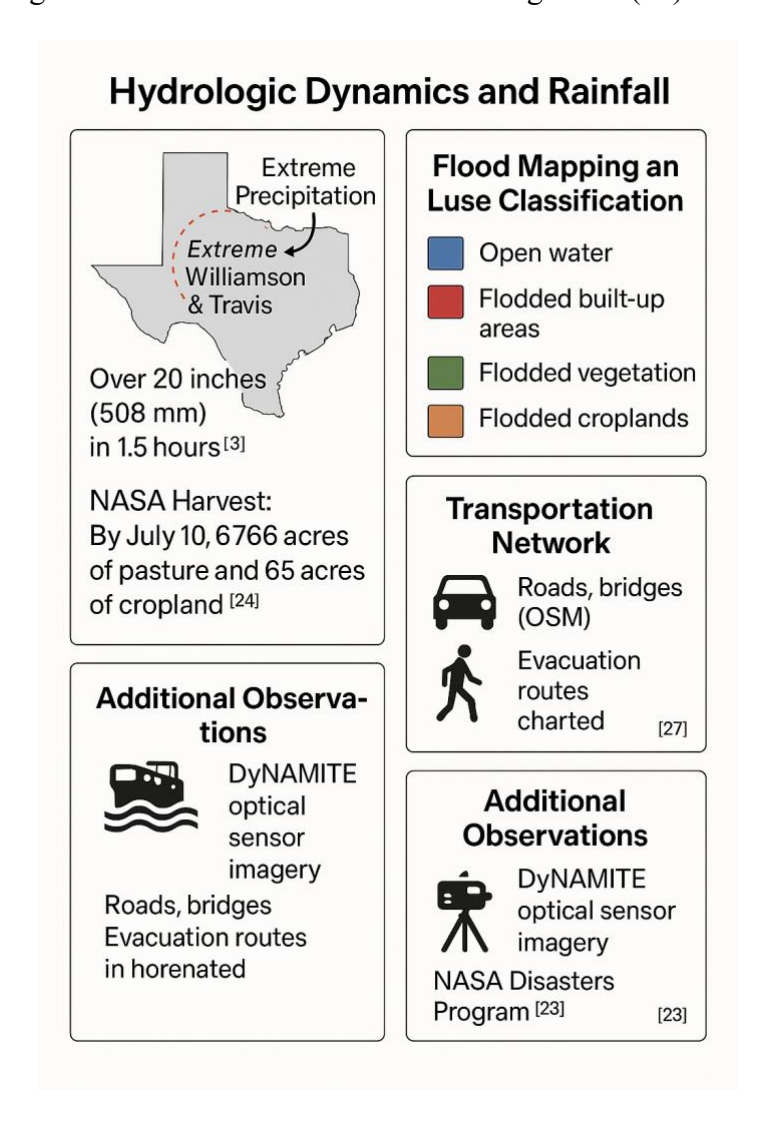
Hydrologic Dynamics and Rainfall

Satellite data (NASA IMERG and NOAA Stage-IV) revealed extreme precipitation in Central Texas during early July 2025. Multi-day rainfall totals exceeded 20 inches (508 mm) near the junction of Burnet, Williamson, and Travis counties. In response to this intense rain, the Guadalupe River rose at catastrophic rates: at Kerrville the river surged by 32 feet (9.8 m) in just 1.5 hours, and downstream at Comfort it rose a similar 32 feet in 1.75 hours. Such rapid water-level rise quickly overflowed riverbanks, washing out bridges and roads and triggering extensive rescue and evacuation operations by federal, state, and local authorities(23). Hundreds of residents were evacuated as flash floodwaters inundated homes and campsites along the river.

Agricultural Impacts

A rapid post-flood assessment by NASA Harvest (RAAPID project) quantified the damage to farmlands in Kerr County. By July 10, 2025 (six days after the flood), about 676 acres of rangeland (0.36% of the county's pasture) and 65 acres of cropland (>9% of all croplands in the county) were inundated(24). While the absolute area of crops lost was small, the relative impact was severe for this predominantly rural area: even short-term flooding can delay planting, reduce

yields, damage farm infrastructure, and strain local livelihoods(24). These rapid satellite-derived estimates proved critical for guiding recovery efforts – local officials could swiftly identify hardest-hit farms and target assistance to affected ranchers and growers(24).



Flood Mapping and Land Use Classification

To map the flood extent, analysts combined observations from multiple radar sensors. Initial water masks from C-band Sentinel-1 imagery (5–20 m resolution) provided a broad overview of inundation, unhindered by clouds or darkness(25). However, to detect flooding hidden under forest canopies and within urban areas, high-resolution L-band UAVSAR airborne data were crucial. NASA's Disaster Program deployed UAVSAR flights on July 9–10, generating 10-m

flood classification maps that differentiated four flood-affected land cover types: open water (blue), flooded built-up areas (red), flooded vegetation (green), and flooded croplands (orange). Non-flooded areas are left transparent in these maps. The use of polarimetric L-band radar allowed distinguishing different scattering mechanisms associated with flooding. For example, inundated forests produce a strong double-bounce return (from water surfaces and upright tree trunks), whereas open floodwater appears dark with weak returns in all polarizations. These maps thus identified not only obvious surface water inundation but also "hidden" flood zones beneath vegetation. (Notably, in urban zones like Austin, buildings oriented along the radar line-of-sight can also create strong double-bounce signals that mimic floods, so such results must be cross-checked with other data.) The flood extent maps produced from UAVSAR and Sentinel-1 were made publicly available via the NASA Disasters Mapping Portal and guided both damage assessment and mitigation planning(23).

Transportation Network and Evacuation Routing

The floods heavily impacted the road network: bridges were damaged or destroyed and many roads submerged, isolating communities and complicating emergency response. A study in npj Natural Hazards underscores that the majority of U.S. flood fatalities occur when people attempt to drive through floodwaters, especially at bridges and low-water crossings(26). To reduce these losses, it is critical to proactively close flooded roadways and provide safe evacuation routes(26). In this event, we developed a "Flood Radar" decision-support system that integrates the SAR-derived flood maps with OpenStreetMap road data and known shelter locations. This system automatically identifies which road segments remain passable and which are cut off by flood or debris, and it charts safe evacuation paths to the nearest shelters (e.g. schools, churches, community centers). It also flags unusable river crossings and bridge outages. By combining near-

real-time flood extent data with transportation networks, such tools can suggest detours and guide evacuees and first responders to safety(26). Furthermore, by integrating up-to-date hydrologic forecasts (e.g. stream gauge forecasts from NOAA's National Water Model) with a bridge inventory, the system can issue site-specific probabilistic flood warnings – essentially predicting which bridges or low crossings are likely to overtop – allowing officials to close those routes ahead of time(26). (See the interactive Flood Radar evacuation map for this Texas event(27).)

Additional Observations

A wealth of satellite and airborne imagery was collected to support response efforts. NASA conducted emergency flights in the week after the flood (July 8–10, 2025), capturing high-resolution optical video (DyNAMITE sensor) and L-band SAR (UAVSAR) over the Guadalupe River Valley(23). These data provided detailed situational awareness: for instance, aerial imagery revealed neighborhoods and infrastructure still inundated or washed away, and pinpointed places where floodwaters had scoured out bridge abutments or undermined highway foundations. Such information prompted immediate engineering inspections and road closures to prevent further accidents. In total, the July 2025 maps showed flooding in numerous communities along the Guadalupe (including Kerrville, Ingram, Hunt, Center Point, and Comfort), as well as along parts of the San Gabriel and Colorado Rivers(23). The combined use of multi-spectral satellite imagery, airborne radar, machine learning, and ground models allowed authorities to rapidly assess the flood's scale and impacts – from agriculture to infrastructure – and to target the most vulnerable areas for evacuation and early recovery efforts.

Discussion

The Central Texas floods of July 2025 demonstrate the value of integrating diverse remote sensing data with models and on-ground information to build a comprehensive situational picture for disaster management.

Multisensor Approach – Advantages

Synthetic Aperture Radar proved especially indispensable, as its all-weather, day-or-night imaging capability meant that flooding could be mapped despite nighttime or heavy storm clouds(25). For instance, the Sentinel-1 C-band satellites (which have a native spatial resolution on the order of 5–20 m(25)) provided timely flood snapshots even during the height of the storm. L-band SAR data (from UAVSAR airborne flights and satellites like JAXA's ALOS-2) complemented these by penetrating deeper into vegetation canopies, using polarimetric signals to detect water beneath forests. Meanwhile, spaceborne precipitation maps from the GPM mission (IMERG) added a dynamic context – delivering global rainfall estimates every 30 minutes at 10 km resolution(18). These rainfall accumulations helped hydrologists identify where intense downpours were likely to produce dangerous runoff surges. Finally, high-resolution digital elevation models (e.g. the 30-m NASA SRTM and ESA Copernicus DEM) were used in hydraulic models (such as HEC-RAS) to simulate floodwave propagation over the terrain. The combination of up-to-date satellite imagery with DEM-informed flood models enabled forecasters to predict how floodwaters might spread and to plan evacuation routes along the least flood-prone corridors.

Challenges and Limitations of SAR Flood Mapping

Despite its strengths, the SAR-based mapping approach faces several technical hurdles. First, speckle noise, the grainy interference pattern inherent to radar images, can obscure fine details and cause false small "flood pixels." Reducing speckle via filtering (multi-looking or spatial averaging) comes at the cost of spatial resolution, potentially blurring or erasing small-scale

features like the double-bounce signals from inundated structures or trees. Advanced speckle reduction techniques or multi-temporal smoothing can help, but must be applied carefully to avoid losing critical flood evidence. Second, the revisit frequency of major SAR satellites is limited. Sentinel-1 operates on a 12-day orbital repeat (per satellite), which improves to ~6 days when both S1A and S1B are functioning. Even so, in many regions a given flood might be captured by only one SAR snapshot or none at all – fast flash floods can rise and recede in a matter of hours or days, well within the gaps of a 6–12 day revisit cycle. In a study of the Ganges Basin, for example, researchers noted that Sentinel-1 data were effectively available only every 12 days, missing much of the flood dynamics(28). New commercial micro-satellite SAR constellations promise much more frequent imaging (even multiple revisits per day) at meter-level resolution, but most offer only a single polarization (usually VV). Lacking cross-polarization data, these images cannot directly exploit polarimetric scattering differences (like double-bounce vs. surface scattering) that were so useful in our analysis. Third, operational flood classification requires extensive preprocessing of the radar data. Steps include orbital correction, radiometric calibration, thermal noise removal, speckle filtering, terrain geocorrection, and conversion of backscatter to a logarithmic scale (dB)(28). Each step must be done correctly to avoid artifacts. Even with proper preprocessing, certain environments pose classification difficulties. In arid or urban areas, for instance, there are surfaces that appear very dark to the radar (e.g. calm water, smooth concrete, or wet asphalt) – all can look like "water" to an algorithm purely based on SAR intensity. This leads to false positives in flood maps. In such cases, analysts have found that combining SAR with optical imagery or LiDAR-derived elevation data can greatly improve reliability, by distinguishing actual water inundation from look-alike dry surfaces. Future approaches will likely employ multisensor data fusion and region-specific model ensembles to refine flood detection in challenging terrains(28).

Early Warning and Institutional Factors

The effectiveness of remote-sensing for disasters ultimately depends on how quickly and broadly its information reaches decision-makers and the public. The July 2025 Texas flood revealed gaps in the "last mile" of alert communication. Despite accurate forecasts and 22 separate flash flood warnings issued by the National Weather Service in the hours before the flood, local authorities in Kerr County failed to activate the regional CodeRED emergency system or sound siren alarms(29). An automated network of flood gauges and sirens had been proposed years prior but was never built - officials had repeatedly rejected funding due to cost and concerns about "noise" in the community(29). As a result, many residents and campers received no notification of the impending deluge and were caught off-guard in the disaster zone. This tragedy underlines that cutting-edge flood maps and predictions have little value if they are not translated into timely, effective warnings on the ground (29)(30). Going forward, the integration of near real-time satellite observations into centralized alerting systems (e.g. using satellite flood maps to trigger geotargeted mobile alerts or highway message signs) could significantly improve dissemination. It is equally critical to invest in resilient communication infrastructure (such as sirens, radio transmitters, and cell networks that stay operational during storms) and to ensure that local agencies trust and act on scientific warnings. In the Texas event, the absence of a robust local warning system turned an extreme weather event into a historic catastrophe. Community education and regular drills are also important so that residents know how to respond when alarms are sounded(29).

Future Outlook

This case points to several directions for improving flood mapping and emergency response. Technical improvements will focus on increasing observation frequency (coordinating across multiple SAR satellites and constellations to achieve near-daily coverage) and on smarter image processing. Speckle noise mitigation could employ adaptive filters or machine-learning techniques that preserve true features while suppressing noise. Likewise, flood classification algorithms may shift toward deep learning model ensembles that account for regional landcover specifics – for example, combining a network tuned for urban settings with another tuned for vegetated floodplains. Data fusion will play a larger role: jointly leveraging SAR, optical, and even LiDAR data to delineate flood boundaries with greater accuracy than any single sensor can achieve. On the emergency management side, automated early warning systems must be developed in tandem with these mapping tools. This includes integrating satellite flood detections, river gauge sensors (IoT), and weather forecasts into a unified platform that can issue alerts or recommend evacuations in real time. Ensuring that local officials and the public are prepared to receive and act on those warnings is equally vital – regular preparedness training, community engagement, and maintained trust in science-based warnings all help translate data into saved lives. Ultimately, the "Flood Radar" approach, blending cutting-edge remote sensing with practical decision support, represents a promising blueprint for minimizing losses in future floods. By continuously advancing the technology and the institutions that use it, we can build more flood-resilient communities in an era of growing climate extremes.

Reference List

- 1. Misra A, White K, Nsutezo SF, Straka W, Lavista J. Mapping global floods with 10 years of satellite radar data. Nature Communications [Internet]. 2025 [cited 2025 Nov 1];16(1). Available from: https://www.nature.com/articles/s41467-025-60973-1.pdf
- 2. The Washington Post. Texas Hill Country is no stranger to flash floods. Why were so many caught off guard? The Washington Post [Internet]. 2025 Jul 6 [cited 2025 Nov 2]; Available from: https://www.washingtonpost.com/weather/2025/07/06/texas-flood-risks-warnings-alerts-preparation/
- 3. Amitrano D, Di Martino G, Di Simone A, Imperatore P. Flood Detection with SAR: A Review of Techniques and Datasets. Remote Sensing [Internet]. 2024 [cited 2025 Nov 2];16(4):656. Available from: https://www.mdpi.com/2072-4292/16/4/656/pdf
- 4. NASA Global Precipitation Measurement (GPM). Global Precipitation Measurement (GPM). NASA; [cited 2025 Nov 1]. IMERG (Integrated Multi-satellite Retrievals for GPM). Available from: https://gpm.nasa.gov/data/imerg
- European Space Agency (ESA). Copernicus Data Space Ecosystem. European Space Agency (ESA); [cited 2025 Nov 1]. Copernicus Digital Elevation Model (COP-DEM). Available from: https://dataspace.copernicus.eu/explore-data/data-collections/copernicus-contributing-missions/collections-description/COP-DEM
- 6. NASA Global Precipitation Measurement (GPM). NASA Global Precipitation Measurement Mission. NASA Goddard Space Flight Center (GES DISC); [cited 2025 Oct 20]. IMERG Early Run 30 minute GES DIS. Available from: https://gpm.nasa.gov/node/2525
- 7. NCAR Climate Data Guide (UCAR). Climate Data Guide. University Corporation for Atmospheric Research (UCAR); [cited 2025 Oct 19]. GPM (Global Precipitation Measurement) Mission. Available from: https://climatedataguide.ucar.edu/climate-data/gpm-global-precipitation-measurement-mission
- 8. Tsutsumida N, Tanaka T, Sultana N. Automated Flood Detection From Sentinel-1 GRD Time Series Using Bayesian Analysis for Change Point Problems. IEEE Transactions on Geoscience and Remote Sensing [Internet]. 2025 [cited 2025 Nov 2];63:1–13. Available from: http://xplorestaging.ieee.org/ielx8/36/10807682/11202584.pdf?arnumber=11202584
- 9. Bentivoglio R, Isufi E, Jonkman SN, Taormina R. Deep learning methods for flood mapping: a review of existing applications and future research directions. Hydrology and Earth System Sciences [Internet]. 2022;26(16):4345–78. Available from: https://hess.copernicus.org/articles/26/4345/2022/
- 10. JAXA Earth Observation Research Center (EORC). JAXA Earth Observation Research Center (EORC). Japan Aerospace Exploration Agency (JAXA); [cited 2025 Oct 23]. PALSAR-2 (Phased Array type L-band Synthetic Aperture Radar-2). Available from: https://www.eorc.jaxa.jp/ALOS-2/en/about/palsar2.htm

- 11. World Meteorological Organization (WMO). OSCAR/Space. World Meteorological Organization (WMO); [cited 2025 Oct 27]. PALSAR-2 (Instrument record). Available from: https://space.oscar.wmo.int/instruments/view/palsar 2
- 12. NASA Airborne Science Program (ASP). NASA Airborne Science Program. NASA; [cited 2025 Oct 28]. Uninhabited Aerial Vehicle Synthetic Aperture Radar (UAVSAR). Available from:
 - https://airbornescience.nasa.gov/instrument/Uninhabited_Aerial_Vehicle_Synthetic_Aperture_Radar
- 13. Salem A, Hashemi-Beni L. Inundated Vegetation Mapping Using SAR Data: A Comparison of Polarization Configurations of UAVSAR L-Band and Sentinel C-Band. Remote Sensing [Internet]. 2022 [cited 2025 Nov 2];14(24):6374. Available from: https://www.mdpi.com/2072-4292/14/24/6374/pdf
- 14. U.S. Geological Survey (USGS). Data.gov. U.S. Geological Survey (USGS); [cited 2025 Oct 29]. Shuttle Radar Topography Mission (SRTM) 1 Arc-Second Global. Available from: https://catalog.data.gov/dataset/shuttle-radar-topography-mission-1-arc-second-global
- 15. Ruth Suehle. Opensource.com. Opensource.com; 2014 [cited 2025 Oct 27]. Using OpenStreetMap to respond to disasters before they happen. Available from: https://opensource.com/life/14/1/openstreetmap-responds-to-disasters
- 16. U.S. Department of Agriculture, National Agricultural Statistics Service (NASS), Disaster Analysis Program. USDA NASS Research & Science Disaster Analysis. U.S. Department of Agriculture (USDA), National Agricultural Statistics Service (NASS); 2025 [cited 2025 Nov 1]. Texas Floods. Available from: https://www.nass.usda.gov/Research_and_Science/Disaster-Analysis/2025/Texas-Floods/2025_July_Texas_Floods_report.pdf
- 17. Travert JP, Goeury C, Boyaval S, Bacchi V, Zaoui F. Evaluating the effects of preprocessing, method selection, and hyperparameter tuning on SAR-based flood mapping and water depth estimation. arXiv preprint arXiv:251011305. 2025;
- 18. NASA Global Precipitation Measurement (GPM). NASA Global Precipitation Measurement Mission. NASA Goddard Space Flight Center; [cited 2025 Nov 1]. What is the spatial and temporal resolution of GPM data? Available from: https://gpm.nasa.gov/node/3176
- 19. Earth Resources Observation and Science (EROS) Center. USGS EROS. U.S. Geological Survey (USGS); 2018 [cited 2025 Oct 28]. USGS EROS Archive Digital Elevation Shuttle Radar Topography Mission (SRTM) 1 Arc-Second Global. Available from: https://www.usgs.gov/centers/eros/science/usgs-eros-archive-digital-elevation-shuttle-radar-topography-mission-srtm-1

- Herfort B, Eckle M, de Albuquerque JP, Zipf A. Towards assessing the quality of volunteered geographic information from OpenStreetMap for identifying critical infrastructures. In: ISCRAM. 2015.
- 21. Gierszewska M, Berezowski T. A Physics-Guided Neural Network for Flooding Area Detection Using SAR Imagery and Local River Gauge Observations. IEEE Journal of Selected Topics in Applied Earth Observations and Remote Sensing [Internet]. 2025 [cited 2025 Nov 2];18:11386–400. Available from: http://xplorestaging.ieee.org/ielx8/4609443/10766875/10967553.pdf?arnumber=10967553
- 22. University of South Florida, Department of Civil & Environmental Engineering. University of South Florida Department of Civil & Environmental Engineering. University of South Florida (USF); [cited 2025 Oct 18]. Hydrologic Engineering Center's River Analysis System (HEC-RAS). Available from: https://www.usf.edu/engineering/cee/faculty-projects/gaim-wbmp/model-library/hec-ras.aspx
- 23. NASA Earth Science Applied Sciences Program Disasters (NASA Disasters Program). NASA Applied Sciences Disasters. NASA; 2025 [cited 2025 Oct 23]. Texas Flooding July 2025. Available from: https://appliedsciences.nasa.gov/what-we-do/disasters/disasters-activations/texas-flooding-july-2025
- 24. NASA Harvest. NASA Harvest. NASA Harvest, University of Maryland; 2025 [cited 2025 Oct 30]. Detecting Flood Damage to Agricultural Land in Texas Hill Country. Available from: https://www.nasaharvest.org/news/detecting-flood-damage-to-agricultural-land-intexas-hill-country
- 25. Carre~no Conde F, De Mata Mu~noz M. Flood monitoring based on the study of Sentinel-1 SAR images: The Ebro River case study. Water. 2019;11(12):2454.
- 26. Oh J, Bartos M. Flood early warning system with data assimilation enables site-level forecasting of bridge impacts. npj Natural Hazards [Internet]. 2025 [cited 2025 Nov 2];2(1). Available from: https://www.nature.com/articles/s44304-025-00116-0.pdf
- 27. Antonika Shapovalova. Drypathmap.com. Drypathmap.com; 2025 [cited 2025 Oct 16]. DryPath Presentation (Slide Deck). Available from: https://drypathmap.com/presentationS.pdf
- 28. Sajid M, Khan HH, Khan A, Ahmad R, Khan A, Siraj G, et al. Application of sentinel-1 SAR data for flood monitoring in the lower Ganges Basin: a time-series analysis of 2021 flood in Bihar. Discover Sensors [Internet]. 2025 [cited 2025 Nov 2];1(1). Available from: https://link.springer.com/content/pdf/10.1007/s44397-025-00012-2.pdf
- 29. Farshid Vahedifard, Amir AghaKouchak. United Nations University (UNU) INWEH. United Nations University (UNU); 2025 [cited 2025 Oct 26]. Catastrophic Texas Flood as Science Warned but Sirens Stayed Silent. Available from: https://unu.edu/inweh/article/catastrophic-texas-flood-science-warned-sirens-stayed-silent

30. Faisal Raza. Medium.com. Medium; 2025 [cited 2025 Oct 25]. The Silent Alarm: Kerr County Tragedy and the National Failure of Outdoor Emergency Alert Systems. Available from: https://medium.com/@faisalraza_63848/the-silent-alarm-kerr-county-tragedy-and-the-national-failure-of-outdoor-emergency-alert-systems-a4c1d42155ab